

Article

# Dithienylpyrrole- and Tris[4-(2-thienyl)phenyl]amine-Containing Copolymers as Promising Anodic Layers in High-Contrast Electrochromic Devices

Tzi-Yi Wu \* , Yuh-Shan Su and Jui-Cheng Chang

Department of Chemical Engineering and Materials Engineering, National Yunlin University of Science and Technology, Yunlin 64002, Taiwan; jeff77720@gmail.com (Y.-S.S.); d700215@gmail.com (J.-C.C.)

\* Correspondence: wuty@gmail.yuntech.edu.tw; Tel.: +886-5-534-2601 (ext. 4626)

Received: 22 March 2018; Accepted: 20 April 2018; Published: 27 April 2018



**Abstract:** Three dithienylpyrrole- and tris[4-(2-thienyl)phenyl]amine-containing copolymers (P(MPS-co-TTPA), P(MPO-co-TTPA), and P(ANIL-co-TTPA)) were deposited on indium tin oxide (ITO) surfaces using electrochemical polymerization. Spectroelectrochemical characterizations of polymer films revealed that P(MPS-co-TTPA) film was light olive green, greyish-green, bluish grey, and grey in neutral state, intermediate state, oxidized state, and highly oxidized state, respectively, whereas P(MPO-co-TTPA) film was green moss, foliage green, dark greyish-green, and bluish-grey in neutral state, intermediate state, oxidized state, and highly oxidized state, respectively. The  $\Delta T_{\max}$  of P(MPS-co-TTPA) film at 964 nm, P(MPO-co-TTPA) film at 914 nm, and P(ANIL-co-TTPA) film at 960 nm were 67.2%, 60.7%, and 67.1%, respectively, and the coloration efficiency ( $\eta$ ) of P(MPS-co-TTPA) film at 964 nm, P(MPO-co-TTPA) film at 914 nm, and P(ANIL-co-TTPA) film at 960 nm were calculated to be 260.3, 176.6, and 230.8 cm<sup>2</sup> C<sup>-1</sup>, respectively. Dual type complementary colored electrochromic devices (ECDs) were constructed using P(MPS-co-TTPA), P(MPO-co-TTPA), or P(ANIL-co-TTPA) as anodic copolymer layer and PProDOT-Et<sub>2</sub> as cathodic polymer layer. P(MPO-co-TTPA)/PProDOT-Et<sub>2</sub> ECD revealed high  $\Delta T$  (55.1%) and high  $\eta$  (766.5 cm<sup>2</sup> C<sup>-1</sup>) at 580 nm. Moreover, P(MPS-co-TTPA)/PProDOT-Et<sub>2</sub>, P(MPO-co-TTPA)/PProDOT-Et<sub>2</sub>, and P(ANIL-co-TTPA)/PProDOT-Et<sub>2</sub> ECDs showed satisfactory long-term cycling stability and optical memory.

**Keywords:** electrochemical polymerization; spectroelectrochemistry; electrochromic switching; optical contrast; electrochromic devices

## 1. Introduction

Electrochromic materials have increasingly garnered attention due to their potential applications in low-energy consumption displays, antiglare mirrors, smart windows, and adaptive camouflages [1]. Electrochromic materials are mainly classified as inorganic metal oxides, conjugated polymers, Prussian blue, metal metallohexacyanates, metal phthalocyanines, and viologens [2]. Among these materials, conjugated polymers have been widely investigated due to their satisfactory optical contrast, high coloration efficiency, rapid electrochromic switching speed, multiple color exhibitions, and tunable optical band gap with chemical structure modifications. Recently, conjugated polymers such as polytriphenylamines [3], polycarbazoles [4], polyanilines [5,6], polybenzothiadiazoles [7], polyindoles [8], polythiophenes [9], and polybenzotriazoles [10] have been reported for particular electrochromic behaviors. Among these conjugated polymers, polytriphenylamines and polycarbazoles have hole transport properties and can be oxidized to form stable aminium radical cations, and the

polymer films exhibit distinct color variations during the redox process. Reynolds et al. reported that the optical contrast of multifunctional triphenylamine polymers was up to 45% [11] and Hsiao et al. reported that electroactive polyamides and polyimides containing trityl-triphenylamine units revealed good thermal stability and a green-blue or blue coloring variation upon applying potentials, with the  $\Delta T$  between neutral and oxidized states of polymer film up to 84% at 828 nm [12]. Polythiophenes and their derivatives have garnered attention for use in organic electrochromic materials due to their special optical and electrochemical characteristics such as low band gap and reversibility of the redox processes. Moreover, each repeat unit of poly(2,5-dithienylpyrrole)s (PSNS) incorporated a pyrrole ring between two thiophene units, which gave rise to decreases in the onset potential of polymer films. The incorporation of alkyl and alkoxy groups to the nitrogen atom of central pyrrole unit in PSNS backbone gave rise to good solubility of PSNS in general solvents and tunable band gap of PSNS [13]. Koyuncu et al. reported a new low band gap electrochromic polymer (poly(SNSC-BSe)) consisting of 2,5-dithienylpyrrole, carbazole, and 2,1,3-benzoselenadiazole units; the poly(SNSC-BSe) film showed a high contrast ratio (51%) in the near-infrared region, a high coloration efficiency ( $274 \text{ cm}^2 \text{ C}^{-1}$ ), and retained 94.6% of its electrochemical activity after 1000 cycles [14]. Soganci et al. synthesized two amide-substituted poly(dithienylpyrrole)s (P(PBA) and P(PBA-co-EDOT)) and reported their multichromic behaviors: P(PBA-co-EDOT) displayed low band gap (1.67 eV), high optical contrast (77% at 1000 nm), and high coloration efficiency ( $697.01 \text{ cm}^2 \text{ C}^{-1}$ ) [15]. Furthermore, copolymers supply effectual ways for modulating the electrochromic properties of conjugated polymers, thereby combining or changing the electrochromic behaviors of individual homopolymers. Camurlu et al. [16] reported the optoelectronic performances of poly(2,5-dithienylpyrrole)s with fluorophore units, which were namely PSNS-Carb and PSNS-Flo. PSNS-Carb showed yellow to blue upon doping and displayed an optical contrast of 27.78%. Two copolymers (P(SNS-Carb-co-EDOT) and P(SNS-Flo-co-EDOT)) were also synthesized electrochemically: P(SNS-Carb-co-EDOT) displayed a wide range of colors upon oxidation (ruby, orange, yellow, green, blue, and gray), whereas P(SNS-Flo-co-EDOT) showed several colors from boysenberry to orange, yellow, green, blue, and gray. Moreover, the optical contrast and coloration efficiency of P(SNS-Carb-co-EDOT) and P(SNS-Flo-co-EDOT) were higher than those of PSNS-Carb and PSNS-Flo, respectively.

In this study, three 2,5-dithienylpyrrole- and tris(4-(thiophen-2-yl)phenyl)amine-based copolymers (P(MPS-co-TTPA), P(MPO-co-TTPA), and P(ANIL-co-TTPA)) were copolymerized electrochemically. The chemical structure of 1-(4-(methylthio)phenyl)-2,5-di(thiophen-2-yl)-pyrrole (MPS) is similar to 1-(4-methoxyphenyl)-2,5-di(thiophen-2-yl)-pyrrole (MPO) and 4-(2,5-di(thiophen-2-yl)-pyrrol-1-yl)benzotrile (ANIL). Methylthio-phenyl, methoxy-phenyl, and cyano-phenyl were incorporated to the central pyrrole rings of MPS, MPO, and ANIL units, respectively. The methylthio-phenyl and methoxy-phenyl groups are electron-donating units in MPS and MPO, respectively, whereas the cyano-phenyl group is an electron-withdrawing unit in ANIL. The highest occupied molecular orbital (HOMO) level, lowest unoccupied molecular orbital (LUMO) level, and band gap of PSNS can be modulated using various electron-donating and electron-withdrawing units. Moreover, tris(4-(thiophen-2-yl)phenyl)amine (TTPA) with a triphenylamine unit as the core and three thiophene units as the arms has attracted increasing attention due to its high stability to electrochemical redox reaction and electrochromic switching [17]. The electron-donating triphenylamine unit decreases the oxidation potential of the entire TTPA. Accordingly, poly(TTPA) shows lower  $E_{\text{onset}}$  than that of polythiophenes. It was interesting to combine the TTPA unit and SNS derivatives in copolymer backbones and investigate the electrochromic characteristics of copolymer films. Moreover, the electrochromic devices (ECDs) were fabricated using P(MPS-co-TTPA), P(MPO-co-TTPA), or P(ANIL-co-TTPA) as the anodic coloring electrode, PProDOT-Et<sub>2</sub> as the complementary counter electrode, and an ionic liquid/poly(vinylidene fluoride-co-hexafluoropropylene) (PVDF-HFP) composite film as the electrochromic electrolyte. The percent transmittance variations, coloration efficiency, long-term cycling stability, and open-circuit memory of ECDs were comprehensively explored.

## 2. Materials and Methods

### 2.1. Materials and Electrochemical Preparation of Polymer Electrodes

Dithienylpyrrole derivatives, TTPA, ProDOT-Et<sub>2</sub>, and 1-ethyl-3-propylimidazolium bis(trifluoromethanesulfonyl)imide ([EPI<sup>+</sup>][TFSI<sup>-</sup>]) were synthesized based on previously published procedures [18–21]. P(MPS-co-TTPA), P(MPO-co-TTPA), and P(ANIL-co-TTPA) films were electrosynthesized potentiostatically at 1.0 V on ITO surfaces with a charge density of 30 mC cm<sup>-2</sup>. The reference electrode used in the preparation of the polymers is an Ag/AgCl electrode. The active area of copolymer films on ITO surfaces was 1.8 cm<sup>2</sup>. P(MPS-co-TTPA), P(MPO-co-TTPA), and P(ANIL-co-TTPA) films were electrosynthesized using feed molar ratios of MPS/TTPA, MPO/TTPA, and ANIL/TTPA, respectively, at 1/1. PProDOT-Et<sub>2</sub> film was coated onto ITO surfaces at +1.4 V.

### 2.2. Fabrication of ECDs

Electrochromic electrolyte was prepared using a mixture containing ionic liquid ([EPI<sup>+</sup>][TFSI<sup>-</sup>]), poly(vinylidene fluoride-co-hexafluoropropene) (PVDF-HFP), propylene carbonate, and dimethylformamide organic solvent [22]. Dual-type ECDs were framed using P(MPS-co-TTPA), P(MPO-co-TTPA), or P(ANIL-co-TTPA) film as the anodic electrode material and PProDOT-Et<sub>2</sub> as the cathodic electrode material. The anodic and cathodic polymer films were positioned to face each other and were separated by an electrochromic electrolyte, as shown in Figure 1.

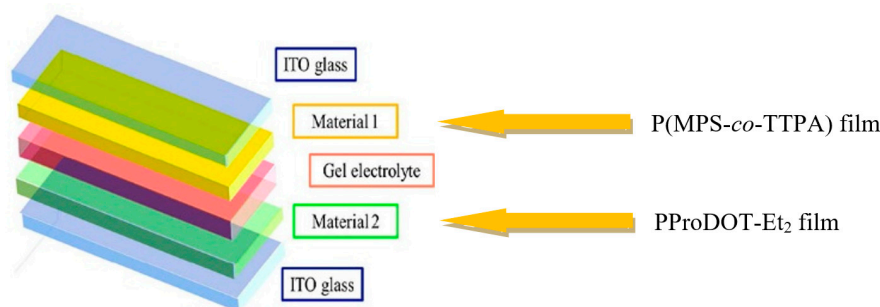


**Figure 1.** Schemes of a P(MPS-co-TTPA)/PProDOT-Et<sub>2</sub> electrochromic device.

### 2.3. Spectroelectrochemical Characterizations of Copolymer Films and ECDs

Spectroelectrochemical properties of copolymer films and ECDs were measured using a CHI660a electrochemical analyzer (CH Instruments, Austin, TX, USA) and a V-630 JASCO UV-Visible spectrophotometer (JASCO International Co., Ltd., Tokyo, Japan). Copolymer films were characterized in a three-component system, copolymer films coated on ITO glass plate were used as working electrodes, a platinum wire and an Ag/AgCl electrode were used as counter and reference electrodes, respectively.

## 3. Results and Discussion

### 3.1. Preparation of Copolymer Films

The CV curves of neat TTPA, MPS, MPO, and ANIL monomers, and the mixtures of two monomers (TTPA + MPS, TTPA + MPO, and TTPA + ANIL) in 0.1 M LiClO<sub>4</sub>/ACN solution are presented in Figure 2. The homopolymer and copolymer films can be clearly seen with continuously increasing cycles, indicating the formation of homopolymer and copolymer films on the ITO glass surface during the electrocoating process [23].

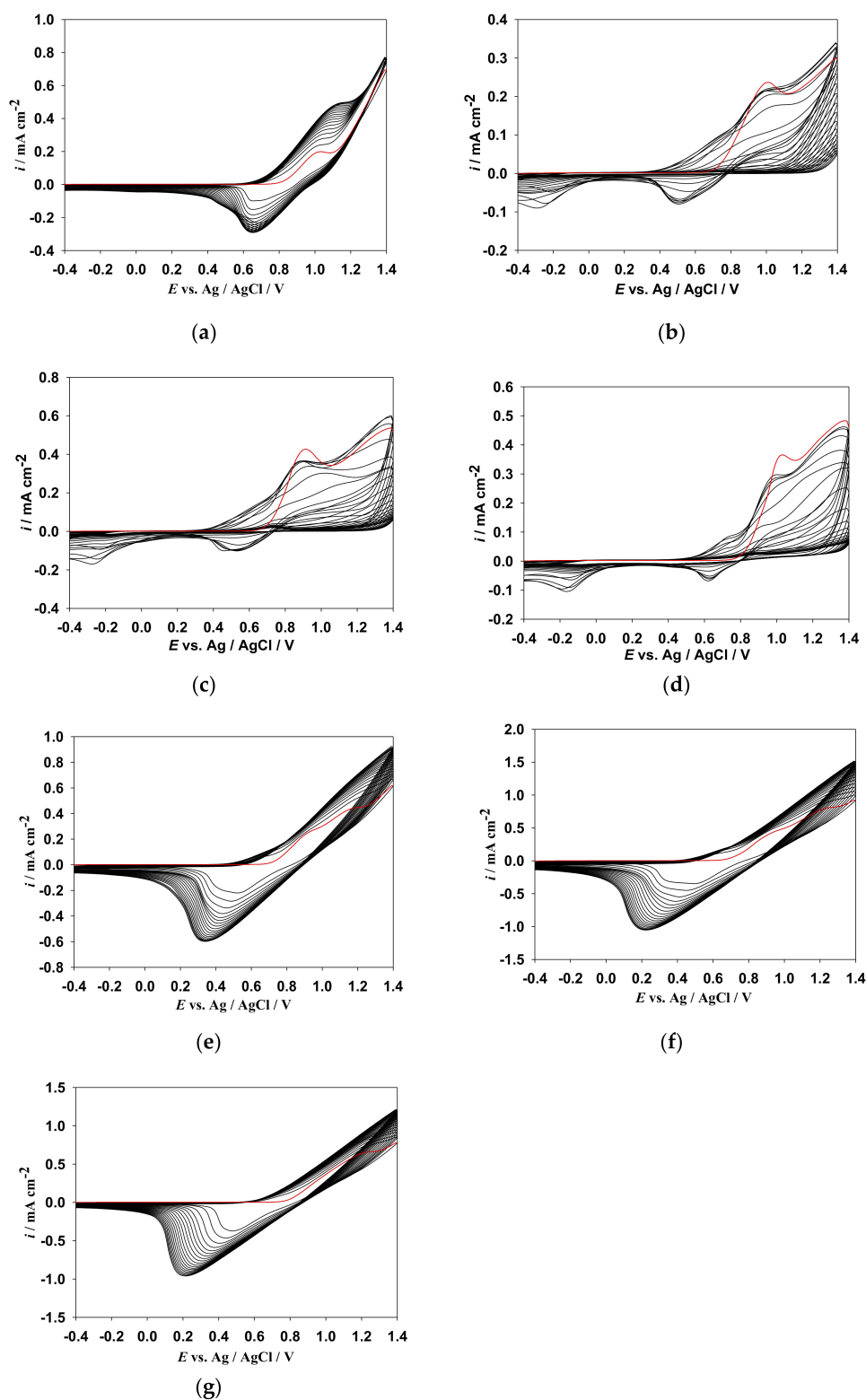


**Figure 2.** Cyclic voltammograms of (a) 2 mM TTPA; (b) 2 mM MPS; (c) 2 mM MPO; (d) 2 mM ANIL; (e) 1 mM TTPA + 1 mM MPS; (f) 1 mM TTPA + 1 mM MPO and (g) 1 mM TTPA + 1 mM ANIL in 0.1 M  $\text{LiClO}_4/\text{ACN}$  at a scan rate of  $100 \text{ mV s}^{-1}$ . TTPA: tris(4-(thiophen-2-yl)phenyl)amine; MPS: 1-(4-(methylthio)phenyl)-2,5-di(thiophen-2-yl)-pyrrole; MPO: 1-(4-methoxyphenyl)-2,5-di(thiophen-2-yl)-pyrrole; ANIL: 4-(2,5-di(thiophen-2-yl)-pyrrol-1-yl)benzotrile.

As presented in Figure 2, the  $E_{\text{onset}}$  of TTPA, MPS, MPO, ANIL, TTPA + MPS, TTPA + MPO, and TTPA + ANIL are 0.79, 0.70, 0.69, 0.81, 0.72, 0.70, and 0.78 V, respectively. The onset potential disparities of TTPA vs. MPS, TTPA vs. MPO, and TTPA vs. ANIL are less than 0.1 V, indicating the feasibility of copolymerization using TTPA and dithienylpyrrole monomers [24]. The onset oxidation potential of P(ANIL-co-TTPA) is greater than those of P(MPS-co-TTPA) and P(MPO-co-TTPA); this can be attributed to an electron-donating methylthio substituent in a MPS unit and an electron-donating methoxy substituent in a MPO unit decreasing the onset oxidation potential with respect to that of a cyano-containing ANIL unit. The oxidation peaks of PTTPA, PMPS, PMPO, PANIL, P(MPS-co-TTPA), P(MPO-co-TTPA), and P(ANIL-co-TTPA) films were 1.16, 0.95, 0.9, 1.0, 1.12, 1.21, and 1.19 V, respectively, whereas the reduction peaks of PTTPA, PMPS, PMPO, PANIL, P(MPS-co-TTPA), P(MPO-co-TTPA), and P(ANIL-co-TTPA) films were 0.66, 0.5, 0.55, 0.6, 0.34, 0.21, and 0.22 V, respectively, as shown in Table 1. The wave shapes and redox peaks of cyclic voltammograms (CVs) observed for P(MPS-co-TTPA), P(MPO-co-TTPA), and P(ANIL-co-TTPA) films are different to those of PTTPA, PMPS, PMPO, and PANIL films, proving the formation of P(MPS-co-TTPA), P(MPO-co-TTPA), and P(ANIL-co-TTPA) films. The electrochemical schemes of P(MPS-co-TTPA) are presented in Figure 3.

**Table 1.** The onset potentials, oxidation potentials, and reduction potentials values of copolymer films.

Polymer Films	Onset Potentials/V	Oxidation Potentials/V	Reduction Potentials/V
P(MPS-co-TTPA)	0.72	1.12	0.34
P(MPO-co-TTPA)	0.70	1.21	0.21
P(ANIL-co-TTPA)	0.78	1.19	0.22

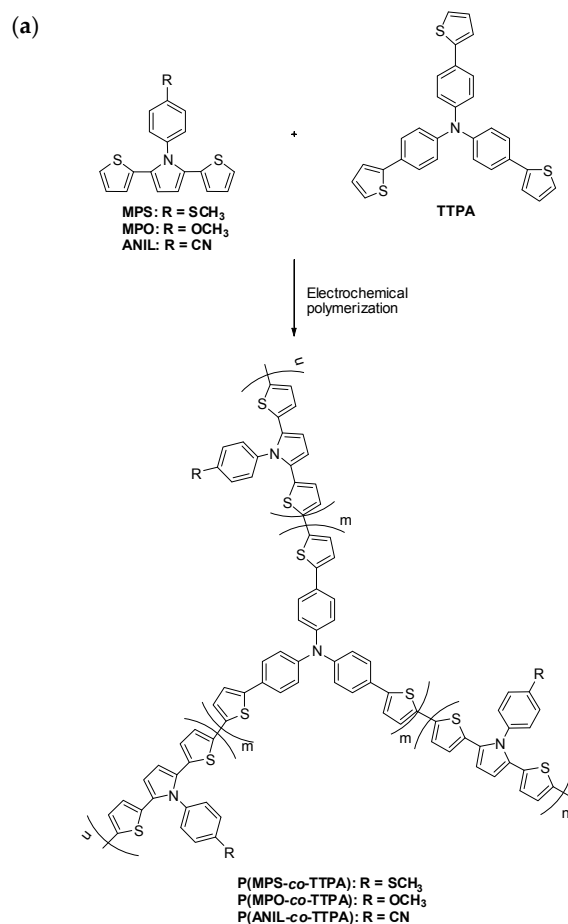


**Figure 3.** Cont.

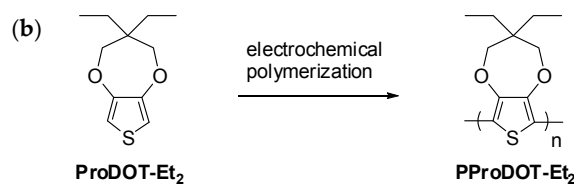


**Figure 3.** The electrochemical copolymerization schemes of (a) anodic copolymers (P(MPS-*co*-TTPA), P(MPO-*co*-TTPA), and P(ANIL-*co*-TTPA)) and (b) cathodic polymer PProDOT-Et<sub>2</sub>.

The as-prepared P(MPS-*co*-TTPA), P(MPO-*co*-TTPA), and P(ANIL-*co*-TTPA) films were scanned at 25, 50, 100, 150, 200, and 250  $\text{mV s}^{-1}$  in 0.1 M  $\text{LiClO}_4/\text{ACN}$  solution. As shown in Figure 4a–c, CV curves of P(MPS-*co*-TTPA), P(MPO-*co*-TTPA), and P(ANIL-*co*-TTPA) films displayed distinct oxidation and reduction peaks; the anodic and cathodic peak current densities increased with increasing scan rates, implying that P(MPS-*co*-TTPA), P(MPO-*co*-TTPA), and P(ANIL-*co*-TTPA) films adhered well to the ITO glass electrode. Moreover, Figure 4d–f shows linear relationships between peak current densities and scan rates, illustrating that the reduction-oxidation processes of P(MPS-*co*-TTPA), P(MPO-*co*-TTPA), and P(ANIL-*co*-TTPA) films were not restricted by diffusion control [25].

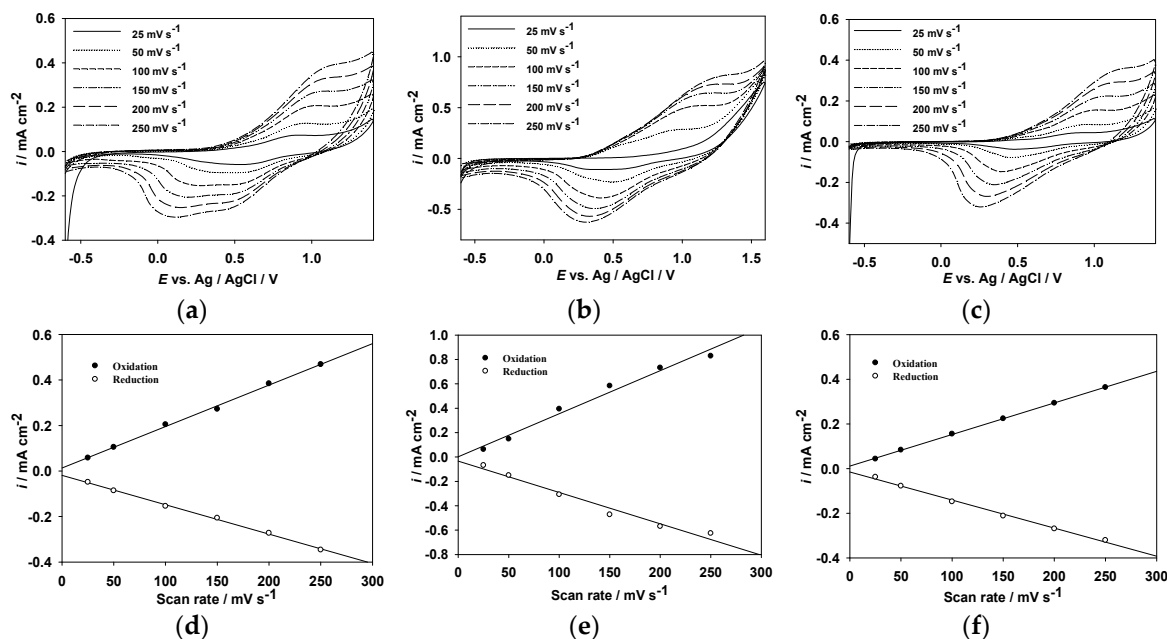


**Figure 4.** CV curves of (a) P(MPS-*co*-TTPA); (b) P(MPO-*co*-TTPA); and (c) P(ANIL-*co*-TTPA) films at various scan rates between 25 and 250  $\text{mV s}^{-1}$  in 0.1 M  $\text{LiClO}_4/\text{ACN}$  solution. Their corresponding relationships of peak current density vs. scan rate of (d) P(MPS-*co*-TTPA); (e) P(MPO-*co*-TTPA); and (f) P(ANIL-*co*-TTPA) films in 0.1 M  $\text{LiClO}_4/\text{ACN}$  solution.

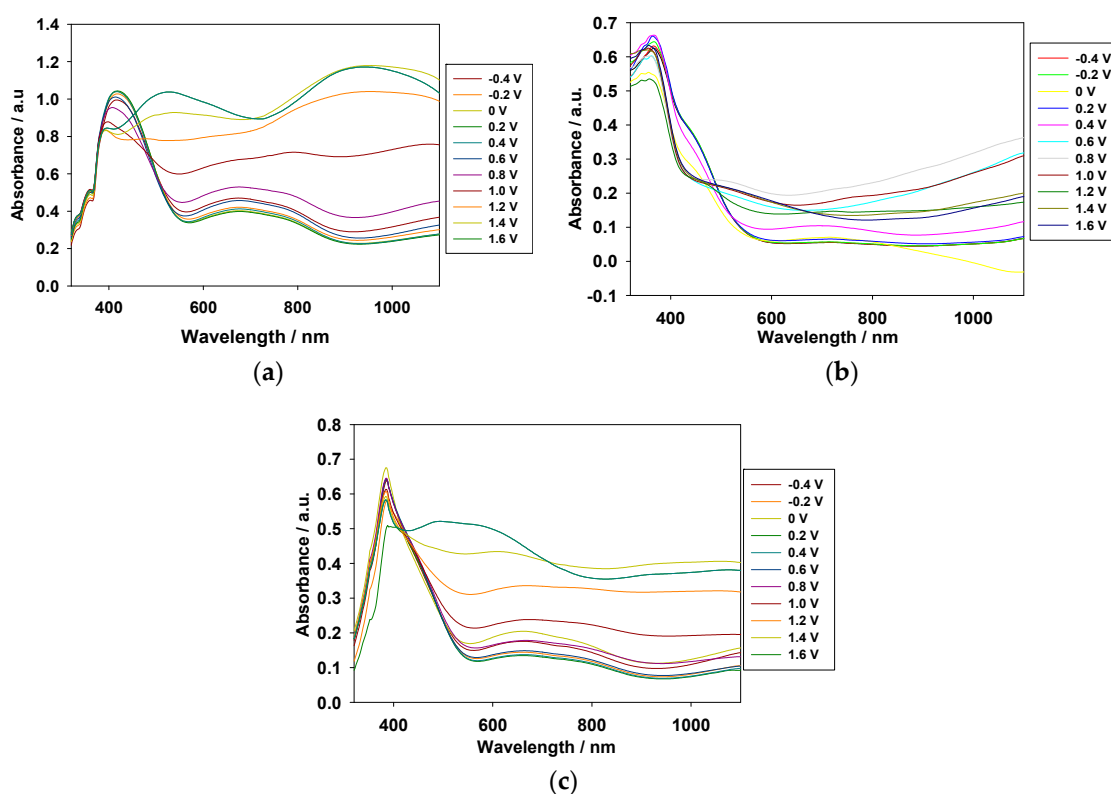
### 3.2. Spectroelectrochemical Studies of Copolymer Films

The spectroelectrochemical investigations of P(MPS-*co*-TTPA), P(MPO-*co*-TTPA), and P(ANIL-*co*-TTPA) films coated on ITO surfaces were carried out in  $[\text{EPI}^+][\text{TFSI}^-]$  solution. As displayed in Figure 5, the absorption peaks of P(MPS-*co*-TTPA), P(MPO-*co*-TTPA), and P(ANIL-*co*-TTPA) films were found at 417, 369, and 385 nm, respectively, in their neutral state, which indicated the  $\pi-\pi^*$  transition of P(MPS-*co*-TTPA), P(MPO-*co*-TTPA), and P(ANIL-*co*-TTPA) in  $[\text{EPI}^+][\text{TFSI}^-]$  solution. Upon applying potentials more than 1.2 V, the peaks of P(MPS-*co*-TTPA), P(MPO-*co*-TTPA), and P(ANIL-*co*-TTPA) films at 417, 369, and 385 nm, respectively, decreased little by little and their charge carrier absorption bands appeared at 964, 914, and 960 nm, respectively, implying the formation of

polaron and bipolaron of copolymer films [26]. The band gap energy values ( $E_g$ ) of PMPS, PMPO, PANIL, PTTTPA, P(MPS-co-TTPA), P(MPO-co-TTPA), and P(ANIL-co-TTPA) can be calculated according to the following Planck equation [27,28],

$$E_g = 1241/\lambda_{\text{onset}} \quad (1)$$

where  $\lambda_{\text{onset}}$  is the wavelength at which the onset of absorption occurs. The  $E_g$  of PMPS, PMPO, PANIL, PTTTPA, P(MPS-co-TTPA), P(MPO-co-TTPA), and P(ANIL-co-TTPA) were 2.25, 2.17, 2.21, 2.31, 2.27, 2.22, and 2.28 eV, respectively. P(MPO-co-TTPA) showed a narrower band gap than those of P(MPS-co-TTPA) and P(ANIL-co-TTPA); this can be attributed to PMPO showing a narrower band gap than those of PMPS and PANIL.



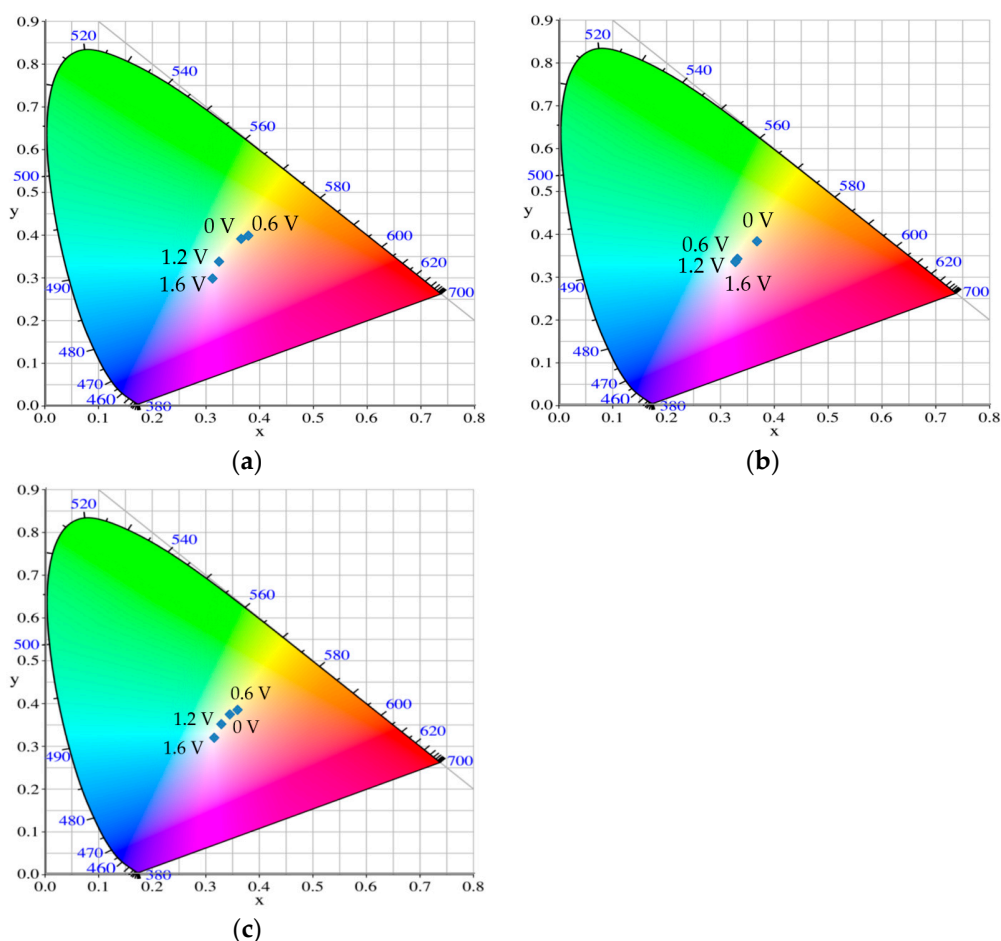
**Figure 5.** UV-Vis spectra of (a) P(MPS-co-TTPA); (b) P(MPO-co-TTPA); and (c) P(ANIL-co-TTPA) films at various potentials.

Table 2 and Table S1 (in Supplementary Information) show the electrochromic photographs and colorimetric values, respectively, of P(MPS-co-TTPA), P(MPO-co-TTPA), and P(ANIL-co-TTPA) films at various potentials in solutions. P(MPS-co-TTPA) film was light olive green (0 V) in the neutral state, greyish-green (+0.6 V) in the intermediate state, bluish grey (+1.2 V) in oxidized state, and grey (+1.6 V) in highly oxidized state. P(MPO-co-TTPA) film was green moss at 0 V, foliage green at +0.6 V, dark greyish-green at +1.2 V, and bluish-grey at +1.6 V. However, P(ANIL-co-TTPA) film showed less color variations than those of P(MPS-co-TTPA) and P(MPO-co-TTPA) films; P(ANIL-co-TTPA) film was lawn green at 0, +0.6 V, and +1.2 V, and celandine green at +1.6 V—this may be attributed to P(ANIL-co-TTPA) film revealing higher onset potential of oxidation than those of (MPS-co-TTPA) and P(MPO-co-TTPA) films and an electron-withdrawing cyano unit deactivating the  $\pi$ - $\pi^*$  transitions of benzene ring on the pyrrole ring of P(ANIL-co-TTPA). The Commission Internationale de l'Éclairage (CIE) chromaticity diagrams of P(MPS-co-TTPA), P(MPO-co-TTPA), and P(ANIL-co-TTPA) films at various potentials are shown in Figure 6: the ( $x,y$ ) values of P(MPO-co-TTPA) film showed significant

variations before 0.6 V, whereas the  $(x,y)$  values of P(MPS-co-TTPA) and P(ANIL-co-TTPA) films showed significant variations after 0.6 V.

**Table 2.** Electrochromic behaviors of copolymer films at various voltages.

Polymer Films	0 V	0.6 V	1.2 V	1.6 V
P(MPS-co-TTPA)				
P(MPO-co-TTPA)				
P(ANIL-co-TTPA)				



**Figure 6.** CIE chromaticity diagrams of (a) P(MPS-co-TTPA); (b) P(MPO-co-TTPA); and (c) P(ANIL-co-TTPA) films in neutral and oxidation states.

The switching kinetics of P(MPS-co-TTPA), P(MPO-co-TTPA), and P(ANIL-co-TTPA) films were measured using a square-wave potential step technology [29]. P(MPS-co-TTPA), P(MPO-co-TTPA), and P(ANIL-co-TTPA) films were stepped by repeated potential between  $-0.2$  and  $+0.9$  V in an ionic liquid solution, with the time interval of 5 s. Figure 7 shows the time-dependent changes in the

transmittance profiles of P(MPS-*co*-TTPA), P(MPO-*co*-TTPA), and P(ANIL-*co*-TTPA) films in solution state, and the transmittance changes ( $\Delta T$ ) measured at 1st, 50th, and 100th cycles are listed in Table 3. The  $\Delta T_{\max}$  of P(MPS-*co*-TTPA) film at 964 nm, P(MPO-*co*-TTPA) film at 914 nm, and P(ANIL-*co*-TTPA) film at 960 nm were 67.0%, 60.7%, and 66.4%, respectively, at the first cycle. Among these copolymer films, P(MPS-*co*-TTPA) film at 964 nm shows the highest  $\Delta T$ . The coloring respond time ( $\tau_c$ ) and the bleaching respond time ( $\tau_b$ ) of copolymer films measured at 1st, 50th, and 100th cycles are also presented in Table 3. The  $\tau_c$  and  $\tau_b$  were determined at 90% of the full-transmittance changes and were in the range of 1.82–2.21 s for P(MPS-*co*-TTPA), P(MPO-*co*-TTPA), and P(ANIL-*co*-TTPA) films.

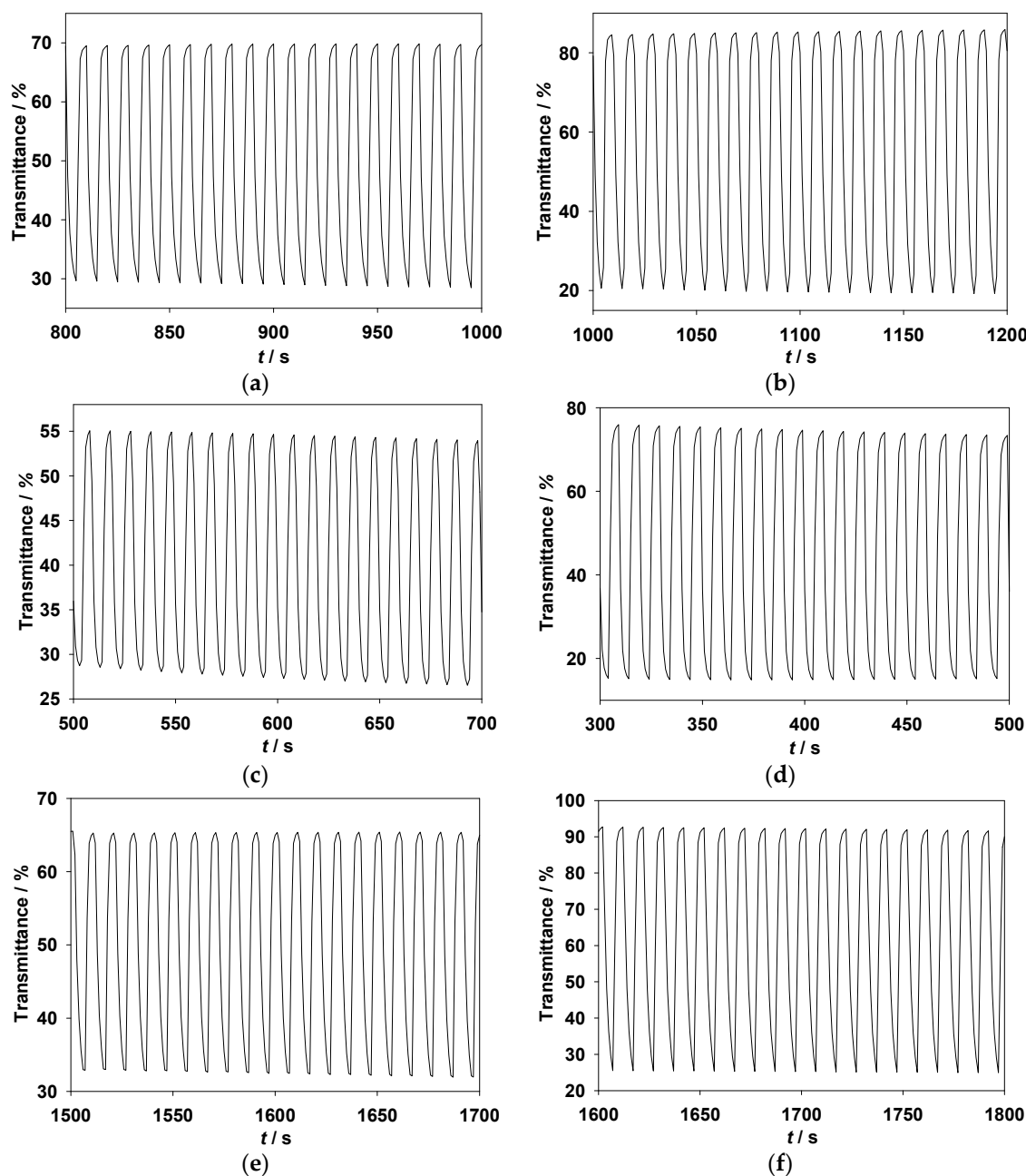


**Figure 7.** In situ transmittance of (a) P(MPS-*co*-TTPA) at 570 nm; (b) P(MPS-*co*-TTPA) at 964 nm; (c) P(MPO-*co*-TTPA) at 592 nm; (d) P(MPO-*co*-TTPA) at 914 nm; (e) P(ANIL-*co*-TTPA) at 548 nm; and (f) P(ANIL-*co*-TTPA) at 960 nm as a function of time in solution state, with the time interval of 5 s. The copolymer films were stepped by repeated potential between  $-0.2$  and  $+0.9$  V.

**Table 3.** Color–bleach switching properties of copolymer films in solution state.

Polymer Films in [EPI <sup>+</sup> ][TFSI <sup>-</sup> ]	$\lambda_{\max}/\text{nm}$	Cycle No.	$\Delta T/\%$	$\tau_c/s$	$\tau_b/s$
				$T_{90\%}$	$T_{90\%}$
P(MPS- <i>co</i> -TTPA)	570	1	39.47	2.05	1.85
		50	40.82	2.16	1.88
		100	39.35	2.21	2.02
	964	1	67.04	2.06	1.90
		50	66.68	2.16	1.82
		100	67.18	2.21	1.84
P(MPO- <i>co</i> -TTPA)	592	1	25.74	2.02	1.90
		50	26.09	2.04	1.95
		100	25.57	2.12	2.01
	914	1	60.69	1.99	1.93
		50	58.06	2.01	1.96
		100	56.23	1.97	1.91
P(ANIL- <i>co</i> -TTPA)	548	1	32.43	2.19	1.87
		50	31.45	2.15	1.97
		100	32.37	2.14	1.82
	960	1	66.38	2.17	1.96
		50	66.27	2.18	1.87
		100	67.08	2.11	1.85

$\Delta OD$  can be determined using the following equation [30]:

$$\Delta OD = \log\left(\frac{T_{\text{ox}}}{T_{\text{neu}}}\right) \quad (2)$$

where  $T_{\text{ox}}$  and  $T_{\text{neu}}$  are the transmittance of the oxidation state and neutral state, respectively. The  $\Delta OD$  of P(MPS-*co*-TTPA) film at 964 nm, P(MPO-*co*-TTPA) film at 914 nm, and P(ANIL-*co*-TTPA) film at 960 nm in solution states are 66.5%, 69.7%, and 55.9%, respectively.

The coloration efficiency ( $\eta$ ) of P(MPS-*co*-TTPA), P(MPO-*co*-TTPA), and P(ANIL-*co*-TTPA) films can be calculated using the following equation [31]:

$$\eta = \frac{\Delta OD}{q/A} \quad (3)$$

where  $q$  and  $A$  are the consumed charge and electrode area, respectively. The  $\eta$  of P(MPS-*co*-TTPA) film at 964 nm, P(MPO-*co*-TTPA) film at 914 nm, and P(ANIL-*co*-TTPA) film at 960 nm were 260.3, 176.6, and 230.8  $\text{cm}^2 \text{C}^{-1}$ , respectively.

Table 4 summarizes the comparisons of  $\Delta T$  and  $\eta$  for several polymer films. The  $\Delta T$  of P(MPS-*co*-TTPA), P(MPO-*co*-TTPA), and P(ANIL-*co*-TTPA) films in solution state were higher than those reported for P(TPVB-*co*-EDOT) film [32] at 555 nm, P(SNS-PN-*co*-EDOT) film [33] at 480 nm, and P(SNS-PN-*co*-ProDOT) film [34] at 850 nm. In another aspect, the  $\eta$  of P(MPS-*co*-TTPA) film in solution state was higher than those reported for P(SNS-PN-*co*-ProDOT) film [34] at 850 nm.

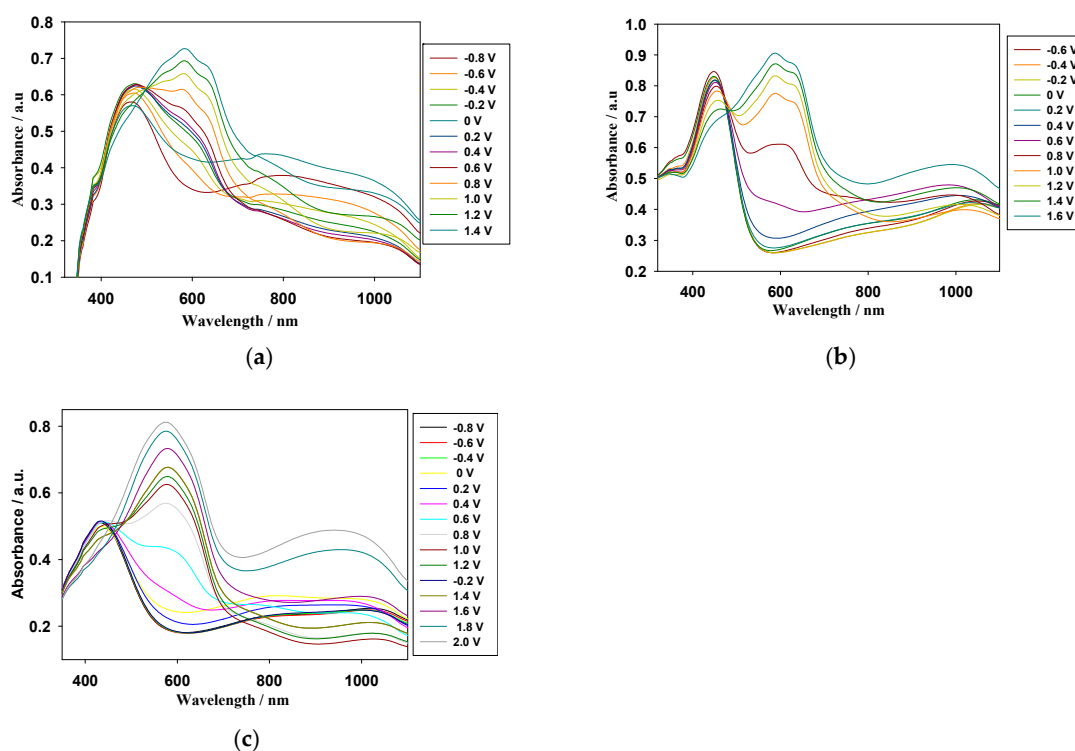
### 3.3. Spectroelectrochemistry of Dual Type ECDs

Figure 8 shows the spectroelectrochemical spectra of ECDs at various potentials. P(MPS-*co*-TTPA)/PProDOT-Et<sub>2</sub>, P(MPO-*co*-TTPA)/PProDOT-Et<sub>2</sub>, and P(ANIL-*co*-TTPA)/PProDOT-Et<sub>2</sub> ECDs displayed absorption peaks at ca. 430 nm at  $-0.4$  V, which is in keeping with the spectra of P(MPS-*co*-TTPA), P(MPO-*co*-TTPA), and P(ANIL-*co*-TTPA) films at  $-0.4$  V. In the aforementioned circumstances, the cathodic PProDOT-Et<sub>2</sub> layer is in oxidized state and it does not reveal conspicuous absorption peak in UV-Vis spectra. Upon increasing the voltage progressively, P(MPS-*co*-TTPA), P(MPO-*co*-TTPA), and

P(ANIL-*co*-TTPA) films start to oxidize and the PProDOT-Et<sub>2</sub> film starts to reduce, new absorption bands at ca. 580 nm emerge, and the ECDs are blue at +1.4 V, as shown in Table 5. The colorimetric values of ECDs at various potentials are summarized in Table S2 (in Supplementary Information), and the CIE chromaticity diagrams of P(MPS-*co*-TTPA)/PProDOT-Et<sub>2</sub>, P(MPO-*co*-TTPA)/PProDOT-Et<sub>2</sub>, and P(ANIL-*co*-TTPA)/PProDOT-Et<sub>2</sub> ECDs at various potentials are shown in Figure 9.

**Table 4.** Comparisons of transmittance changes and coloration efficiencies of polymer films.

Polymer Films	Electrolyte	$\lambda/\text{nm}$	$\Delta T_{\text{max}}/\%$	$\Delta OD_{\text{max}}/\%$	$\eta_{\text{max}}/\text{cm}^2 \text{C}^{-1}$	Ref.
P(TPVB- <i>co</i> -EDOT)	0.1 M TBP <sub>6</sub> /DCM	555	44	–	–	[32]
P(TPVB- <i>co</i> -EDOT)	0.1 M TBP <sub>6</sub> /DCM	1000	75	–	–	[32]
P(SNS-PN- <i>co</i> -EDOT)	0.1 M NaClO <sub>4</sub> /LiClO <sub>4</sub> /ACN	480	8	–	–	[33]
P(SNS-PN- <i>co</i> -ProDOT)	0.1 M LiClO <sub>4</sub> /ACN	850	42	–	256.0	[34]
P(MPS- <i>co</i> -TTPA)	[EPI <sup>+</sup> ][TFSI <sup>-</sup> ]	964	67.2	66.5	260.3	This work
P(MPO- <i>co</i> -TTPA)	[EPI <sup>+</sup> ][TFSI <sup>-</sup> ]	914	60.7	69.7	176.6	This work
P(ANIL- <i>co</i> -TTPA)	[EPI <sup>+</sup> ][TFSI <sup>-</sup> ]	960	67.1	55.9	230.8	This work



**Figure 8.** Spectroelectrochemical spectra of (a) P(MPS-*co*-TTPA)/PProDOT-Et<sub>2</sub>; (b) P(MPO-*co*-TTPA)/PProDOT-Et<sub>2</sub>; and (c) P(ANIL-*co*-TTPA)/PProDOT-Et<sub>2</sub> electrochromic devices (ECDs).

The time-dependent changes in the transmittance profiles of P(MPS-*co*-TTPA)/PProDOT-Et<sub>2</sub>, P(MPO-*co*-TTPA)/PProDOT-Et<sub>2</sub>, and P(ANIL-*co*-TTPA)/PProDOT-Et<sub>2</sub> ECDs are presented in Figure 10, which were switched square wave potentials between  $-0.4$  and  $+1.4$  V with a time interval of 5 s, and the  $\Delta T$  and switching time estimated at various cycles are listed in Table 6. The transmittance changes of P(MPS-*co*-TTPA)/PProDOT-Et<sub>2</sub>, P(MPO-*co*-TTPA)/PProDOT-Et<sub>2</sub>, and P(ANIL-*co*-TTPA)/PProDOT-Et<sub>2</sub> ECDs are 49.21% at 576 nm, 55.12% at 580 nm, and 46.34% at 582 nm at the first cycle, respectively, indicating that P(MPS-*co*-TTPA), P(MPO-*co*-TTPA), and P(ANIL-*co*-TTPA) films are promising electrochromic materials to increase the  $\Delta T$  when we use P(MPS-*co*-TTPA), P(MPO-*co*-TTPA), and P(ANIL-*co*-TTPA) films as electrode materials in ECDs. For the  $\tau_c$  and  $\tau_b$  of ECDs, the switching time of ECDs were shorter than those of P(MPS-*co*-TTPA), P(MPO-*co*-TTPA),

and P(ANIL-co-TTPA) films in solution state, implying that the ECDs changed color faster at various potentials than the copolymer films in solution state.

**Table 5.** Electrochromic behaviors of ECDs at various voltages.

ECDs	0 V	0.6 V	1.0 V	1.4 V
P(MPS-co-TTPA)/PProDOT-Et <sub>2</sub>				
P(MPO-co-TTPA)/PProDOT-Et <sub>2</sub>				
P(ANIL-co-TTPA)/PProDOT-Et <sub>2</sub>				

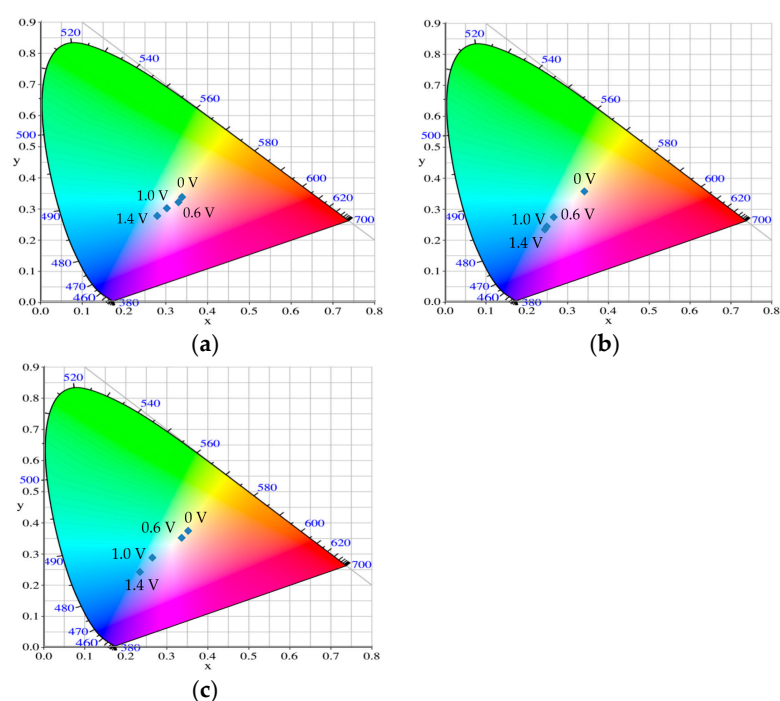


**Figure 9.** CIE chromaticity diagrams of (a) P(MPS-co-TTPA)/PProDOT-Et<sub>2</sub>; (b) P(MPO-co-TTPA)/PProDOT-Et<sub>2</sub>; and (c) P(ANIL-co-TTPA)/PProDOT-Et<sub>2</sub> ECDs.

**Table 6.** Color-bleach switching properties of ECDs.

ECDs	$\lambda_{\max}/\text{nm}$	Cycle No.	$\Delta T/\%$	$\tau$ /s	
				$T_{95\%}$	$T_{95\%}$
P(MPS-co-TTPA)/PProDOT-Et <sub>2</sub>	576	1	49.21	1.01	0.93
		50	49.53	1.01	0.96
		100	48.89	1.14	0.97
P(MPO-co-TTPA)/PProDOT-Et <sub>2</sub>	580	1	55.12	0.98	0.99
		50	54.12	1.01	0.99
		100	53.60	1.05	1.13
P(ANIL-co-TTPA)/PProDOT-Et <sub>2</sub>	582	1	46.34	1.17	1.34
		50	45.76	0.98	1.25
		100	44.91	1.17	1.32

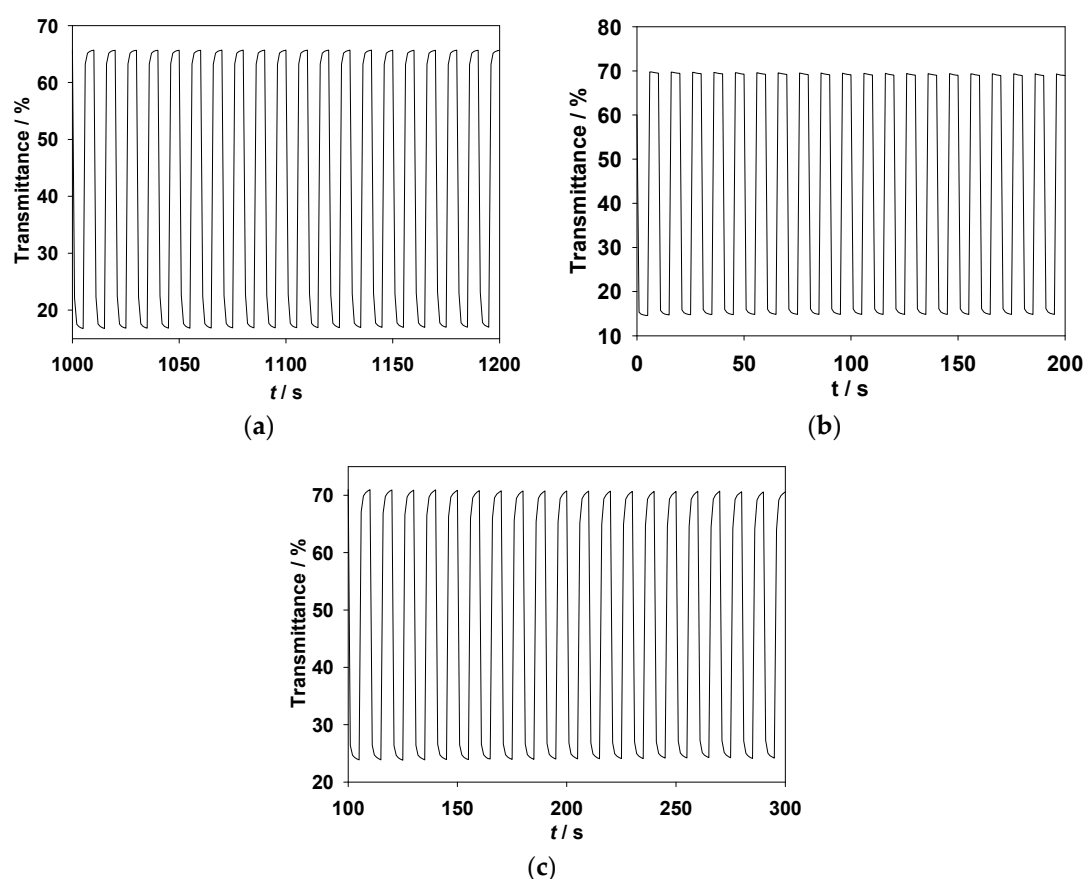


**Figure 10.** In situ transmittance of (a) P(MPS-*co*-TTPA)/PProDOT-Et<sub>2</sub>; (b) P(MPO-*co*-TTPA)/PProDOT-Et<sub>2</sub>; and (c) P(ANIL-*co*-TTPA)/PProDOT-Et<sub>2</sub> ECDs as a function of time, with the time interval of 5 s. The ECDs were stepped by repeated potential between  $-0.4$  and  $+1.4$  V.

Table 7 shows the comparisons of  $\Delta T$  and  $\eta$  for P(MPS-*co*-TTPA)/PProDOT-Et<sub>2</sub>, P(MPO-*co*-TTPA)/PProDOT-Et<sub>2</sub>, and P(ANIL-*co*-TTPA)/PProDOT-Et<sub>2</sub> ECDs and reported dual-type ECDs. P(MPS-*co*-TTPA)/PProDOT-Et<sub>2</sub>, P(MPO-*co*-TTPA)/PProDOT-Et<sub>2</sub>, and P(ANIL-*co*-TTPA)/PProDOT-Et<sub>2</sub> ECDs show higher  $\Delta T$  than those reported for P(NTP-*co*-EDOT)/PEDOT [35], P(SNS-An-Fc-*co*-EDOT)/PEDOT [36], P(SNBS-*co*-EDOT)/PEDOT [37], P(PTP-*co*-EDOT)/PEDOT [33], and P(Cz4-*co*-ClIn1)/PProDOT-Me<sub>2</sub> [38] ECDs. On the other hand, P(MPS-*co*-TTPA)/PProDOT-Et<sub>2</sub>, P(MPO-*co*-TTPA)/PProDOT-Et<sub>2</sub>, and P(ANIL-*co*-TTPA)/PProDOT-Et<sub>2</sub> ECDs show higher  $\eta$  than those of P(SNS-An-Fc-*co*-EDOT)/PEDOT [36] and P(Cz4-*co*-ClIn1)/PProDOT-Me<sub>2</sub> [38] ECDs.

**Table 7.** The transmittance changes and coloration efficiency of ECDs.

ECDs	$\lambda/\text{nm}$	$\Delta T_{\text{max}}/\%$	$\Delta \text{OD}_{\text{max}}/\%$	$\eta/\text{cm}^2 \text{C}^{-1}$	Ref.
P(NTP- <i>co</i> -EDOT)/PEDOT	650	23	–	–	[35]
P(SNS-An-Fc- <i>co</i> -EDOT)/PEDOT	601	22	–	484	[36]
P(SNBS- <i>co</i> -EDOT)/PEDOT	485	15	–	–	[37]
P(PTP- <i>co</i> -EDOT)/PEDOT	545	15	–	–	[33]
P(Cz4- <i>co</i> -ClIn1)/PProDOT-Me <sub>2</sub>	575	32	24.6	372.7	[38]
P(MPS- <i>co</i> -TTPA)/PProDOT-Et <sub>2</sub>	576	49.53	60.94	691.2	This work
P(MPO- <i>co</i> -TTPA)/PProDOT-Et <sub>2</sub>	580	55.12	67.58	766.5	This work
P(ANIL- <i>co</i> -TTPA)/PProDOT-Et <sub>2</sub>	582	46.34	45.03	625.4	This work

### 3.4. Optical Memory Effect of ECDs

The optical memory experiment of P(MPS-*co*-TTPA)/PProDOT-Et<sub>2</sub>, P(MPO-*co*-TTPA)/PProDOT-Et<sub>2</sub>, and P(ANIL-*co*-TTPA)/PProDOT-Et<sub>2</sub> ECDs were carried out by imposing potential for 1 s for each 200 s time interval. The monitor potentials for P(MPS-*co*-TTPA)/PProDOT-Et<sub>2</sub>, P(MPO-*co*-TTPA)/PProDOT-Et<sub>2</sub>, and P(ANIL-*co*-TTPA)/PProDOT-Et<sub>2</sub> ECDs were  $-0.4$  and  $1.0$  V in bleached and colored states, respectively. As shown in Figure S1 (in Supplementary Information), P(MPS-*co*-TTPA)/PProDOT-Et<sub>2</sub>, P(MPO-*co*-TTPA)/PProDOT-Et<sub>2</sub>, and P(ANIL-*co*-TTPA)/PProDOT-Et<sub>2</sub> ECDs showed less than 1.5% transmittance change in bleached state ( $-0.4$  V) and less than 4% transmittance change in colored state ( $1.0$  V), thus inferring that ECDs that employed P(MPS-*co*-TTPA), P(MPO-*co*-TTPA), and P(ANIL-*co*-TTPA) as anodic layers displayed satisfactory optical memory effects.

### 3.5. Redox Stability of ECDs

Long-term redox stabilities of P(MPS-*co*-TTPA)/PProDOT-Et<sub>2</sub>, P(MPO-*co*-TTPA)/PProDOT-Et<sub>2</sub>, and P(ANIL-*co*-TTPA)/PProDOT-Et<sub>2</sub> ECDs were estimated by CV measurements for one thousand cycles at a scan rate of  $100 \text{ mV s}^{-1}$ . As presented in Figure 11, 96%, 93%, and 95%, respectively, of electrochemical activity was maintained for P(MPS-*co*-TTPA)/PProDOT-Et<sub>2</sub>, P(MPO-*co*-TTPA)/PProDOT-Et<sub>2</sub>, and P(ANIL-*co*-TTPA)/PProDOT-Et<sub>2</sub> ECDs after 500 cycles, and 90%, 90%, and 92%, respectively, of electrochemical activity was retained after 1000 cycles, indicating the ECDs revealed satisfactory long-term redox stability after scanning for 1000 cycles.

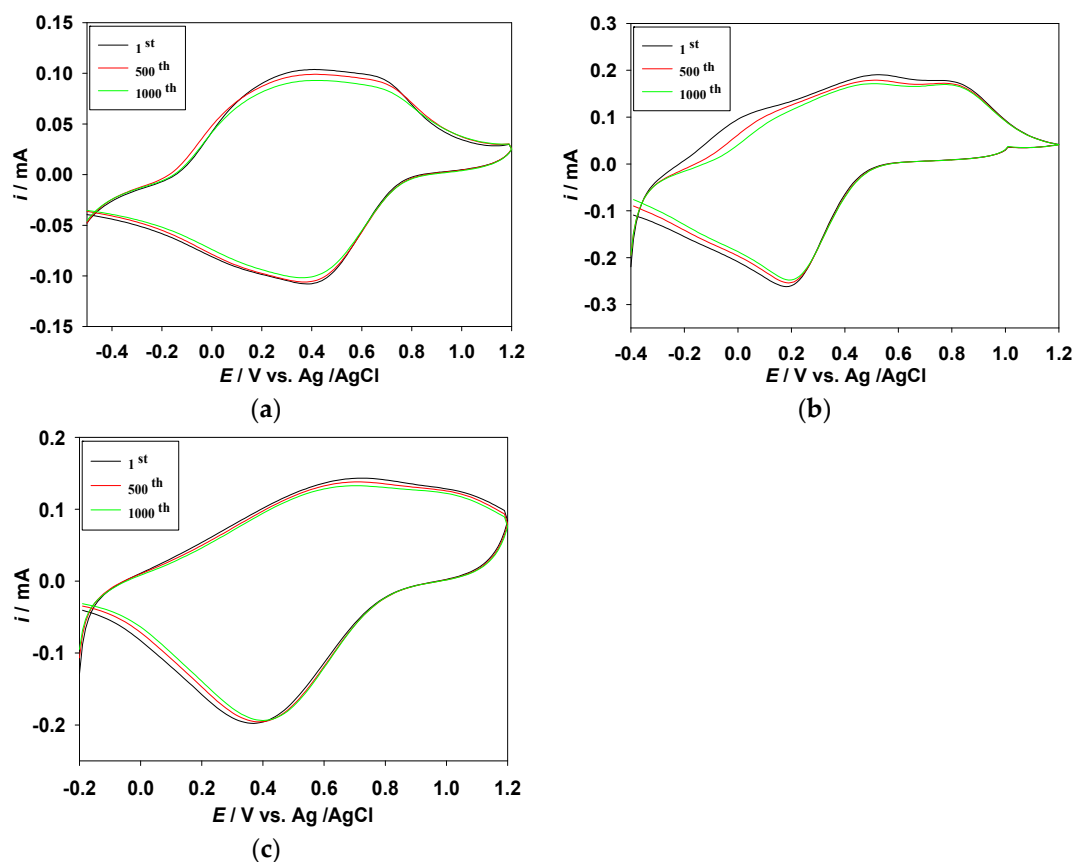


**Figure 11.** Cyclic voltammograms of (a) P(MPS-*co*-TTPA)/PProDOT-Et<sub>2</sub>; (b) P(MPO-*co*-TTPA)/PProDOT-Et<sub>2</sub>; and (c) P(ANIL-*co*-TTPA)/PProDOT-Et<sub>2</sub> ECDs as a function of repeated scans at  $100 \text{ mV s}^{-1}$ .

#### 4. Conclusions

P(MPS-*co*-TTPA), P(MPO-*co*-TTPA), and P(ANIL-*co*-TTPA) films were synthesized electrochemically and characterized in [EPI<sup>+</sup>][TFSI<sup>-</sup>] solution. Spectroelectrochemical investigations revealed that P(MPS-*co*-TTPA) film was light olive green, greyish-green, bluish grey, and grey at 0, 0.6, 1.2, and 1.6 V, respectively. P(MPS-*co*-TTPA) and P(MPO-*co*-TTPA) films showed four kinds of color variations from neutral state to highly oxidized state. Color-bleach switching characterizations of polymer films revealed that P(MPS-*co*-TTPA) film has high  $\Delta T_{\max}$  (67.2% at 964 nm) and high  $\eta$  (260.3 cm<sup>2</sup> C<sup>-1</sup> at 964 nm). The  $\Delta T$  of P(MPS-*co*-TTPA), P(MPO-*co*-TTPA), and P(ANIL-*co*-TTPA) films in an ionic liquid solution were higher than those reported for P(TPVB-*co*-EDOT), P(SNS-PN-*co*-EDOT), and P(SNS-PN-*co*-ProDOT) films. Dual type complementary colored ECDs that employed polymer films as anodic and cathodic layers were constructed; the switching time of ECDs were shorter than those of corresponding copolymer films in [EPI<sup>+</sup>][TFSI<sup>-</sup>] solution. P(MPS-*co*-TTPA)/PProDOT-Et<sub>2</sub> ECDs revealed high  $\Delta T$  (49.5%) and high  $\eta$  (691.2 cm<sup>2</sup> C<sup>-1</sup>) at 576 nm, whereas P(MPO-*co*-TTPA)/PProDOT-Et<sub>2</sub> ECDs displayed reasonable switching time and satisfactory electrochromic memory. P(MPS-*co*-TTPA)/PProDOT-Et<sub>2</sub>, P(MPO-*co*-TTPA)/PProDOT-Et<sub>2</sub>, and P(ANIL-*co*-TTPA)/PProDOT-Et<sub>2</sub> ECDs showed higher  $\Delta T$  than those reported for P(NTP-*co*-EDOT)/PEDOT, P(SNS-An-Fc-*co*-EDOT)/PEDOT, P(SNBS-*co*-EDOT)/PEDOT, P(PTP-*co*-EDOT)/PEDOT, and P(Cz4-*co*-CIn1)/PProDOT-Me<sub>2</sub> ECDs. In view of the above electrochromic properties, P(MPS-*co*-TTPA), P(MPO-*co*-TTPA), and P(ANIL-*co*-TTPA) films could be employed as the anodic layers in ECDs.

**Supplementary Materials:** The following are available online at <http://www.mdpi.com/2079-6412/8/5/164/s1>, Table S1: Colorimetric values of the copolymer films at various potentials in solution state; Table S2: Colorimetric values of ECDs at various potentials; Figure S1: Open circuit stability of (a) P(MPS-*co*-TTPA)/PProDOT-Et<sub>2</sub> ECD monitored at 576 nm, (b) P(MPO-*co*-TTPA)/PProDOT-Et<sub>2</sub> ECD monitored at 580 nm, and (c) P(ANIL-*co*-TTPA)/PProDOT-Et<sub>2</sub> ECD monitored at 582 nm.

**Author Contributions:** Y.-S.S., J.-C.C., and T.-Y.W. conceived the research topic, implemented the experiments, and analyzed the electrochromic properties.

**Acknowledgments:** The authors would like to thank the Ministry of Science and Technology (MOST) of the Republic of China for financially supporting this project.

**Conflicts of Interest:** The authors declare no conflict of interest.

#### References

1. Beaujuge, P.M.; Reynolds, J.R. Color control in  $\pi$ -conjugated organic polymers for use in electrochromic devices. *Chem. Rev.* **2010**, *110*, 268–320. [[CrossRef](#)] [[PubMed](#)]
2. Mortimer, R.G. Electrochromic materials. *Chem. Soc. Rev.* **1997**, *26*, 147–156. [[CrossRef](#)]
3. Hsiao, S.-H.; Lu, H.-Y. Electrosynthesis of aromatic poly(amide-amine) films from triphenylamine-based electroactive compounds for electrochromic applications. *Polymers* **2017**, *9*, 708. [[CrossRef](#)]
4. Su, Y.-S.; Wu, T.-Y. Three carbazole-based polymers as potential anodically coloring materials for high-contrast electrochromic devices. *Polymers* **2017**, *9*, 284. [[CrossRef](#)]
5. Tian, Y.; Zhang, X.; Dou, S.; Zhang, L.; Zhang, H.; Lv, H.; Wang, L.; Zhao, J.; Li, Y. A comprehensive study of electrochromic device with variable infrared emissivity based on polyaniline conducting polymer. *Sol. Energy Mater. Sol. Cells* **2017**, *170*, 120–126. [[CrossRef](#)]
6. Kuo, C.W.; Chen, B.K.; Li, W.B.; Tseng, L.Y.; Wu, T.Y.; Tseng, C.G.; Chen, H.R.; Huang, Y.C. Effects of supporting electrolytes on spectroelectrochemical and electrochromic properties of polyaniline-poly(styrene sulfonic acid) and poly(ethylenedioxythiophene)-poly(styrene sulfonic acid)-based electrochromic device. *J. Chin. Chem. Soc.* **2014**, *61*, 563–570. [[CrossRef](#)]
7. Beaujuge, P.M.; Vasilyeva, S.V.; Liu, D.Y.; Ellinger, S.; McCarley, T.D.; Reynolds, J.R. Structure-performance correlations in spray-processable green dioxothiophene-benzothiadiazole donor-acceptor polymer electrochromes. *Chem. Mater.* **2012**, *24*, 255–268. [[CrossRef](#)]
8. Kuo, C.W.; Wu, T.Y.; Huang, M.W. Electrochromic characterizations of copolymers based on 4,4'-bis(*N*-carbazolyl)-1,1'-biphenyl and indole-6-carboxylic acid and their applications in electrochromic devices. *J. Taiwan Inst. Chem. Eng.* **2016**, *68*, 481–488. [[CrossRef](#)]

9. Lin, K.; Zhang, S.; Liu, H.; Zhao, Y.; Wang, Z.; Xu, J. Effects on the electrochemical and electrochromic properties of 3 linked polythiophene derivative by the introduction of polyacrylate. *Int. J. Electrochem. Sci.* **2015**, *10*, 7720–7731.
10. Baran, D.; Balan, A.; Celebi, S.; Esteban, B.M.; Neugebauer, H.; Sariciftci, N.S.; Toppare, L. Processable multipurpose conjugated polymer for electrochromic and photovoltaic applications. *Chem. Mater.* **2010**, *22*, 2978–2987. [[CrossRef](#)]
11. Schmatz, B.; Ponder, J.F., Jr.; Reynolds, J.R. Multifunctional triphenylamine polymers synthesized via direct (hetero) arylation polymerization. *J. Polym. Sci. Part A Polym. Chem.* **2018**, *56*, 147–153. [[CrossRef](#)]
12. Hsiao, S.-H.; Liao, W.-K.; Liou, G.-S. Synthesis and electrochromism of highly organosoluble polyamides and polyimides with bulky trityl-substituted triphenylamine units. *Polymers* **2017**, *9*, 511. [[CrossRef](#)]
13. Su, Y.S.; Chang, J.C.; Wu, T.Y. Applications of three dithienylpyrroles-based electrochromic polymers in high-contrast electrochromic devices. *Polymers* **2017**, *9*, 114. [[CrossRef](#)]
14. Koyuncu, F.B.; Sefer, E.; Koyuncu, S.; Ozdemir, E. A new low band gap electrochromic polymer containing 2,5-bis-dithienyl-1H-pyrrole and 2,1,3-benzoselenadiazole moiety with high contrast ratio. *Polymer* **2011**, *52*, 5772–5779. [[CrossRef](#)]
15. Soganci, T.; Soyleyici, S.; Soyleyici, H.C.; Ak, M. High contrast electrochromic polymer and copolymer materials based on amide-substituted poly(dithienyl pyrrole). *J. Electrochem. Soc.* **2017**, *164*, H11–H20. [[CrossRef](#)]
16. Guven, N.; Camurlu, P. Optoelectronic properties of poly(2,5-dithienylpyrrole)s with fluorophore groups. *J. Electrochem. Soc.* **2015**, *162*, H867–H876. [[CrossRef](#)]
17. Cheng, X.; Zhao, J.; Fu, Y.; Cui, C.; Zhang, X. Electrosynthesis and characterization of a multielectrochromic copolymer of tris[4-(2-thienyl)phenyl]amine with 3,4-ethylenedioxythiophene. *J. Electrochem. Soc.* **2013**, *160*, G6–G13. [[CrossRef](#)]
18. Wu, T.Y.; Su, Y.S. Electrochemical synthesis and characterization of 1,4-benzodioxan-based electrochromic polymer and its application in electrochromic devices. *J. Electrochem. Soc.* **2015**, *162*, G103–G112. [[CrossRef](#)]
19. Cheng, X.; Zhao, J.; Cui, C.; Fu, Y.; Zhang, X. Star-shaped conjugated systems derived from thienyl-derivatized poly(triphenylamine)s as active materials for electrochromic devices. *J. Electroanal. Chem.* **2012**, *677*, 24–30. [[CrossRef](#)]
20. Welsh, D.M.; Kumar, A.; Meijer, E.W.; Reynolds, J.R. Enhanced contrast ratio and rapid switching in electrochromics based on poly(3,4-propylenedioxythiophene) derivatives. *Adv. Mater.* **1999**, *11*, 1379–1382. [[CrossRef](#)]
21. Wu, T.Y.; Chen, B.K.; Hao, L.; Lin, K.F.; Sun, I.W. Thermophysical properties of a room temperature ionic liquid (1-methyl-3-pentyl-imidazolium hexafluorophosphate) with poly(ethylene glycol). *J. Taiwan Inst. Chem. Eng.* **2011**, *42*, 914–921. [[CrossRef](#)]
22. Wu, T.Y.; Liao, J.W.; Chen, C.Y. Electrochemical synthesis, characterization and electrochromic properties of indan and 1,3-benzodioxole-based poly(2,5-dithienylpyrrole) derivatives. *Electrochim. Acta* **2014**, *150*, 245–262. [[CrossRef](#)]
23. Kuo, C.-W.; Chang, J.-K.; Lin, Y.-C.; Wu, T.-Y.; Lee, P.-Y.; Ho, T.-H. Poly(tris(4-carbazoyl-9-ylphenyl)amine)/three poly(3,4-ethylenedioxythiophene) derivatives in complementary high-contrast electrochromic devices. *Polymers* **2017**, *9*, 543. [[CrossRef](#)]
24. Kuo, C.-W.; Lee, P.-Y. Electrosynthesis of copolymers based on 1,3,5-tris(N-carbazoyl)benzene and 2,2'-bithiophene and their applications in electrochromic devices. *Polymers* **2017**, *9*, 518. [[CrossRef](#)]
25. Hsiao, S.-H.; Liao, Y.-C. Facile synthesis of electroactive and electrochromic triptycene poly(ether-imide)s containing triarylamine units via oxidative electro-coupling. *Polymers* **2017**, *9*, 497. [[CrossRef](#)]
26. Kuo, C.-W.; Wu, T.-L.; Lin, Y.-C.; Chang, J.-K.; Chen, H.-R.; Wu, T.-Y. Copolymers based on 1,3-bis(carbazol-9-yl)benzene and three 3,4-ethylenedioxythiophene derivatives as potential anodically coloring copolymers in high-contrast electrochromic devices. *Polymers* **2016**, *8*, 368. [[CrossRef](#)]
27. Wu, T.Y.; Tsao, M.H.; Chen, F.L.; Su, S.G.; Chang, C.W.; Wang, H.P.; Lin, Y.C.; Ou-Yang, W.C.; Sun, I.W. Synthesis and characterization of organic dyes containing various donors and acceptors. *Int. J. Mol. Sci.* **2010**, *11*, 329–353. [[CrossRef](#)] [[PubMed](#)]
28. Tsao, M.H.; Wu, T.Y.; Wang, H.P.; Sun, I.W.; Su, S.G.; Lin, Y.C.; Chang, C.W. An efficient metal free sensitizer for dye-sensitized solar cells. *Mater. Lett.* **2011**, *65*, 583–586. [[CrossRef](#)]

29. Wu, T.-Y.; Chung, H.-H. Applications of tris(4-(thiophen-2-yl)phenyl)amine- and dithienylpyrrole-based conjugated copolymers in high-contrast electrochromic devices. *Polymers* **2016**, *8*, 206. [[CrossRef](#)]
30. Chang, K.H.; Wang, H.P.; Wu, T.Y.; Sun, I.W. Optical and electrochromic characterizations of four 2,5-dithienylpyrrole-based conducting polymer films. *Electrochim. Acta* **2014**, *119*, 225–235. [[CrossRef](#)]
31. Guven, N.; Camurlu, P. Electrosyntheses of anthracene clicked poly(thienylpyrrole)s and investigation of their electrochromic properties. *Polymer* **2015**, *73*, 122–130. [[CrossRef](#)]
32. Soganci, T.; Soyleyici, H.C.; Ak, M.; Cetisli, H. An amide substituted dithienylpyrrole based copolymer: Its electrochromic properties. *J. Electrochem. Soc.* **2016**, *163*, H59–H66. [[CrossRef](#)]
33. Tarkuc, S.; Sahmetlioglu, E.; Tanyeli, C.; Akhmedov, I.M.; Toppare, L. Electrochromic properties of poly (1-(phenyl)-2,5-di(2-thienyl)-1H-pyrrole-co-3,4-ethylenedioxy thiophene) and its application in electrochromic devices. *Opt. Mater.* **2008**, *30*, 1489–1494. [[CrossRef](#)]
34. Bingol, B.E.; Tekin, B.; Carbas, B.B. An investigation on electrochromic properties of new copolymers based on dithienylpyrrole and propylenedioxythiophene. *J. Electroanal. Chem.* **2017**, *806*, 107–115. [[CrossRef](#)]
35. Varis, S.; Ak, M.; Akhmedov, I.M.; Tanyeli, C.; Toppare, L. A novel multielectrochromic copolymer based on 1-(4-nitrophenyl)-2,5-di(2-thienyl)-1H-pyrrole and EDOT. *J. Electroanal. Chem.* **2007**, *603*, 8–14. [[CrossRef](#)]
36. Camurlu, P.; Gültekin, C. A comprehensive study on utilization of *N*-substituted poly(2,5-dithienylpyrrole) derivatives in electrochromic devices. *Sol. Energy Mater. Sol. Cells* **2012**, *107*, 142–147. [[CrossRef](#)]
37. Camurlu, P.; Tarkuc, S.; Sahmetlioglu, E.; Akhmedov, I.M.; Tanyeli, C.; Toppare, L. Multichromic conducting copolymer of 1-benzyl-2,5-di(thiophen-2-yl)-1H-pyrrole with EDOT. *Sol. Energy Mater. Sol. Cells* **2008**, *92*, 154–159. [[CrossRef](#)]
38. Kuo, C.W.; Hsieh, T.H.; Hsieh, C.K.; Liao, J.W.; Wu, T.Y. Electrosynthesis and characterization of four electrochromic polymers based on carbazole and indole-6-carboxylic acid and their applications in high-contrast electrochromic devices. *J. Electrochem. Soc.* **2014**, *161*, D782–D790. [[CrossRef](#)]



© 2018 by the authors. Licensee MDPI, Basel, Switzerland. This article is an open access article distributed under the terms and conditions of the Creative Commons Attribution (CC BY) license (<http://creativecommons.org/licenses/by/4.0/>).